

# Findings from SAFOD studies 2002-2006 most relevant to NSF-EarthScope-0545472 Hadizadeh J., Mair K., DiToro G., and Babaie H.

#### TABLE OF CONTENTS

- 1. The drill site geology
- 2. Subsurface model
- 3. General observatory considerations
- 4. Summary of phase 1 and 2 drilling operations
- **5. Stress measurements**
- 6. Evidence of deformation in SAFOD drill hole
- 7. Studies of ores, cuttings and fluids
- 8. Friction studies
- 9. Samples and sections of set 1, Hadizadeh et al. 2006
  - 9a. summary table of the samples and thin sections
  - 9b. general lithological description of the sampled cores
  - 9c. thin section numbering and labeling format
  - 9d. wrap around map of the sampled cores; thin section locations

#### References

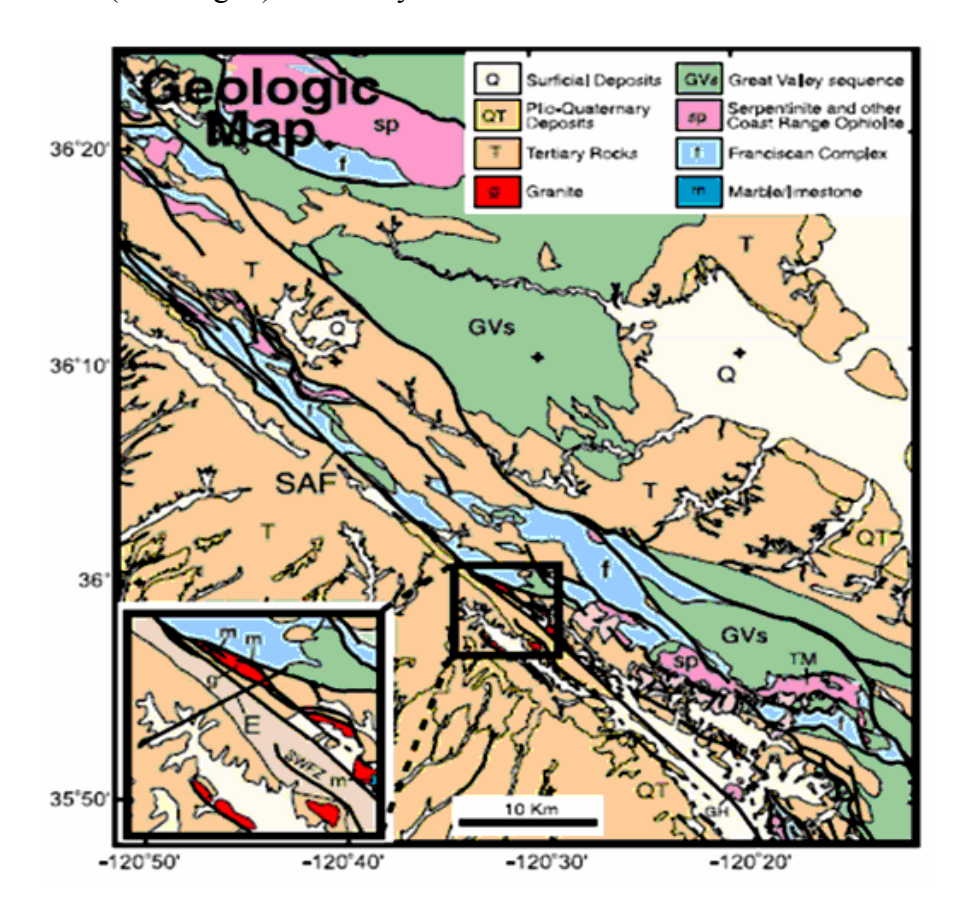
#### **Appendix**

- A1. Characterization recommended to NSF by an international panel
- **A2.** The Franciscan Complex
- A3. Salinian block
- A4. Room temperature friction velocity dependence data
- A5. Resistivity image of the subsurface at the SAFOD site

#### 1. The drill site geology

Geology of the SAFOD drill site in Parkfield area (Fig. 1) is dominated by transpression along the San Andreas Fault (SAF), which has deformed and juxtaposed contrasting rock units. Thayer and Arrowsmith (2005) suggested that the Middle Mountain uplift geological terrain is distinguished by a 1-3 kilometer wide zone of numerous sub-parallel faults and folds. The lithological units either side of the SAF at SAFOD drill site area (inset Fig. 1) are briefly described as follows.

Fig. 1.
Geologic
map of
central
California.
Inset box
shows details
of SAFOD
site at Middle
Mountain.
After Darcy
et al. 2004

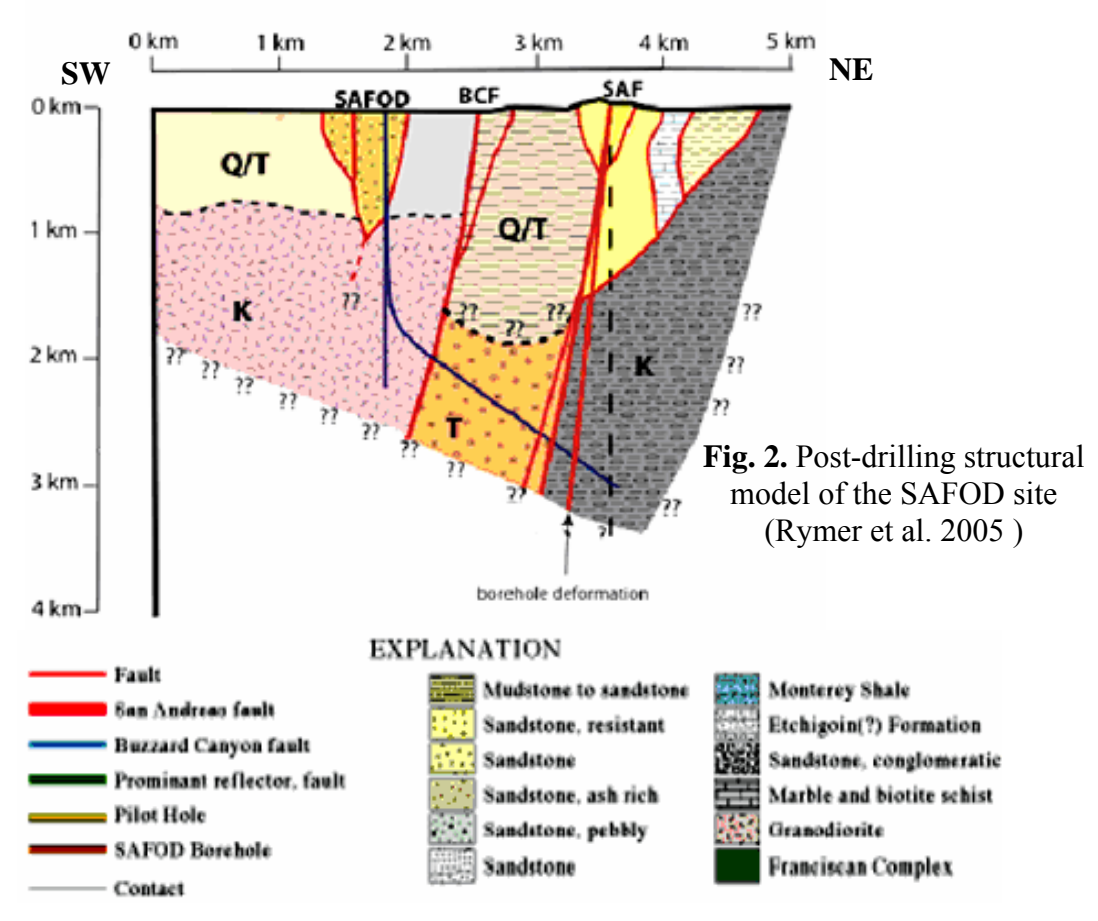


• The northeastern side consists of Miocene to Pliocene marine sedimentary units and Plio-Pleistocene terrestrial sedimentary units. Here, SAF is characterized by Franciscan Complex and their young overlying Great valley sequence rocks (Griscom and Jachens, 1990; Miller et al., 2000). Dominant structures include several high angle faults striking sub-parallel to the main SAF trace that bound marble, granites, and Tertiary sedimentary units. Fault density increases near the active SAF trace. The Gold Hill fault is a reverse fault of varying southwest dip that surfaces along the eastern margin of Middle Mountain and places the Miocene Monterey shale over Pliocene Etchigoin sandstone. Alternating synclines and anticlines with axes trending parallel to the strike of the Gold Hill fault are present within the hanging and foot walls. See Appendix A2 for a petrological description of the Franciscan Complex.

• In the southwestern side an 800 meter thick package of the Plio-Pleistocene Paso Robles Formation is deformed by en echelon folds and secondary faults. Some of the faults strike nearly normal to the SAF, offset Tertiary and Quaternary units, and tend to be northwest-side up. Several SAF-parallel striking faults slice Tertiary and Quaternary sedimentary units and granitic bodies. A fault on the southwestern side of Cholame Creek juxtaposes Tertiary rhyolitic rocks (Pinnacle-Neenach equivalent) against Salinian granite. See Appendix A3 for a petrological description of the Salinian block.

#### 2. Subsurface model

The structure of SAF has been modeled using magnetic, gravity, and geologic data as well as studies of drill core and cuttings (e.g. Roecker et al. 2004, McPhee et al. 2004, Rymer et al. 2005, Hickman 2005). The SAFOD Main Hole (MH) begins vertically 1.8 km SW of the surface trace of the fault and then angles 55° through the fault zone until it passes beneath the surface trace at a depth of 3.2 km. The most recent structural section of the SAF at the drillsite (Fig. 2) suggests that the MH proceeds NE to encounter



at least two fault strands consisting of magnetic granitic rock, serpentinite, or unusually magnetic sandstone. Rymer et al. (2005) and Hickman et al. (2005) suggested that long-term activity of the SAF near the SAFOD site will be concentrated at the contact between the Tertiary arkosic Sst.-conglomerate of the Salinian Formation and the Cretaceous siltstone and shale (Franciscan Complex and its younger sedimentary cover known as

Great Valley Sequence). This boundary lies approximately 600 m SW of the surface trace of the fault. On both sides of this fault contact, several zones exhibit anomalous geophysical properties that may represent several active shear zones. Some of the most dramatic of these are zones about 15 m wide exhibiting low resistivity and low P- and S-wave velocities at measured depths (MD) of 3.07 and 3.16 km. Rock types of the shear zone segment, determined based on loose cuttings (Evans et al. 2005), are consistent with the Great Valley sequence. This suggests that the borehole successfully crossed the SAF, and that the fault zone at depth may contain slivers of Franciscan rocks. Therefore, as is the case along much of the fault in northern California and reflected in regional gravity and magnetic data (Simpson et al.1988, Wentworth et al. 1992), in the Parkfield area SAF juxtaposes Salinian granitic basement on the SW against Franciscan Complex on the NE.

SAF sub-parallel fault density increases three-fold within the overlying sedimentary units, thus confirming that faults bifurcate near the surface (Rymer et al. 2005). Folding of the mid-Tertiary units on the northeast side of fault probably results from SAF-normal compression and movement along the Gold Hill reverse fault. On the other hand, the en echelon folding of the Paso Robles formation on the southwest side of the SAF is consistent with simple shear parallel to the main SAF. The transverse faults on the SW-side of the SAF are most likely high-angle normal faults either developed by SAF-parallel simple shear and later rotated to their current position, or possibly created by slip along a bend in the SAF at depth. Southwestern units are found on the northeastern side of the active trace indicating the ability of the active trace to jump 10s to 100s of meters back to the southwest. Subsurface orientation of faults indicate that the SAF is composed of at least two flower structures in the upper 3 km, with the main trace approximately centered on the more easterly of these structures and a third flower structure farther to the southwest. The flower structures likely merge at depth, but at least in the upper 3 to 4 km (target depth of the SAFOD MH), they are distinct features. Based on inferred ages of rock types juxtaposed across faults and geomorphic evidence along faults Rymer et al. (2005) suggested that the plate boundary (San Andreas fault zone) near the SAFOD site has migrated eastward during the past approximately 20 million years by forming new flower structures.

#### 3. General observatory considerations

Seismotectonic aspects of the Parkfield region (Fig. 3) has made it ideal for the study of small earthquakes and their relationship to tectonic processes; the nucleation region of a repeating magnitude 6 event and a significant portion of the transition from locked to creeping behavior on the San Andreas fault, a relatively well-defined and simple fault segment, and a homogeneous mode of seismic energy release as indicated by the earthquakes.

The observatory consists of retrievable seismic, deformation and environmental sensors deployed inside the casing in both the main hole (maximum temperature 135° C) and the collocated pilot hole (1.1 km depth), and a fiber optic strainmeter installed behind casing in the main hole. These retrievable systems deployed on either wire line or rigid tubing included 15Hz omni-directional and 4.5 Hz gimbaled seismometers, microelectro-mechanical accelerometers, tiltmeters, sigma-delta digitizers, and a fiber optic interferometric strainmeter. Some of the observational highlights include capturing one

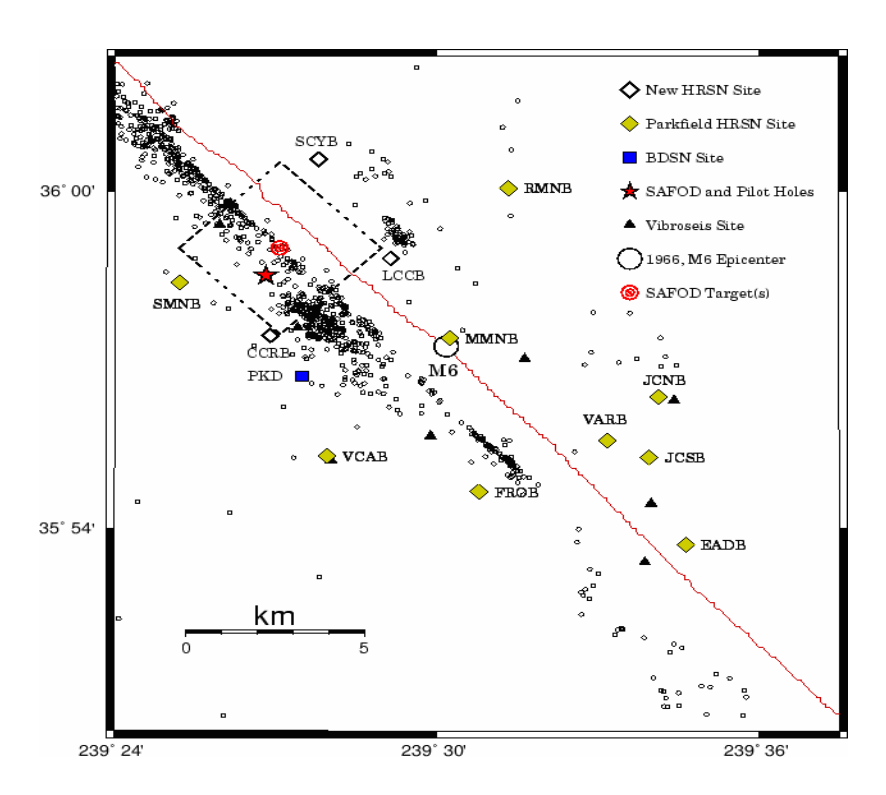


Fig. 3. The seismic monitoring network and the SAF trace (Ellsworth et al. 2005)

of the M2 SAFOD target repeating earthquakes in the near-field at a distance of 420 m, with accelerations of up to 200 cm/s and a static displacement of a few microns. Numerous other local events were observed over the summer by the tilt and seismic instruments in the pilot hole, some of which produced strain offsets of several nano strains on the fiber optic strainmeter. The Northern California Earthquake Data Center at U.C. Berkeley is the principal data repository for SAFOD. The more than 2 TB of 80-level array data are also available at the IRIS DMC as an assembled data collection (Ellsworth et al. 2005). A summary of the characterization recommended to NSF by an international panel is provided in Appendix A1.

#### 4. Summary of Phase 1 and 2 drilling operations

Phase 1: Rotary Drilling to 2.5 km. Drilled 12-1/4"hole to 2.5 km, while collecting continuous drill cuttings and carrying out mud gas analyses. Below 1.5 km, steered hole toward target earthquakes (deviation 55°). Conducted wireline geophysical logging in open hole (electrical and ultrasonic imaging, density, porosity, resistivity, dipole sonic, geochemical, temperature, etc.) After setting casing, obtained 20 m of 4"diameter core at 1.5 and 2.5 km. Conducted permeability tests, fluid sampling and hydrofracsin core holes (Tembe et al. 2006a).

Phase 2: Drilling Through Fault Zone. Drilled inclined 8-1/2 inch diameter hole from 2.5 to 3.1 km. Conducted extensive real-time cuttings and mud gas analyses while drilling across the fault zone. Conducted comprehensive logging while drilling and wireline geophysical logging in open hole. Collected 52 small (0.75"dia. x 1") side-wall cores in open hole. After setting casing, collected 4 m of 2.6 inch diameter spot core at 3.1 km and carried out hydrofracin core hole (Tembe et al. 2006b). See Appendix A5 for

Resistivity image of the subsurface at the SAFOD site showing progression of the phase 1 and 2 drilling operations.

#### 5. Stress measurements

Stress measurements made in the SAFOD pilot hole provide an opportunity to study the relation between crustal stress outside the fault zone and the stress state within it using an integrated mechanical model of a transform fault loaded in transpression. The model proposed by Chery et al. (2004) indicates that only a fault with effective friction as low as 10 times smaller than crustal friction (<0.1) through the seismogenic thickness of the crust is capable of matching stress measurements made in both the far field and in the SAFOD pilot hole (Fig. 4). The stress rotation measured with depth in the SAFOD pilot

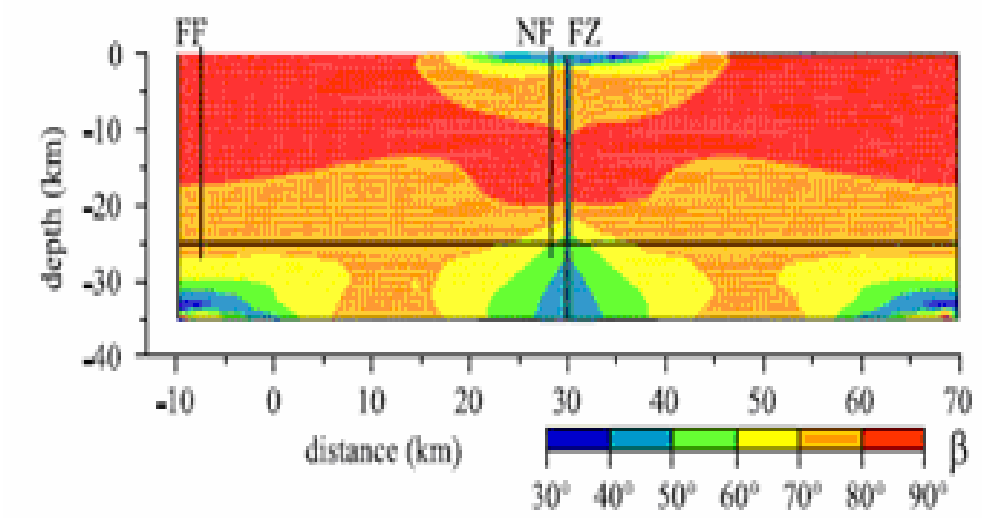


**Fig. 4.** A model of the maximum shear stress orientation with respect to the strike of SAF. FF and NF denote the far field and near filed locations assumed by the model. FZ is the SAF (Chery et al. 2004).

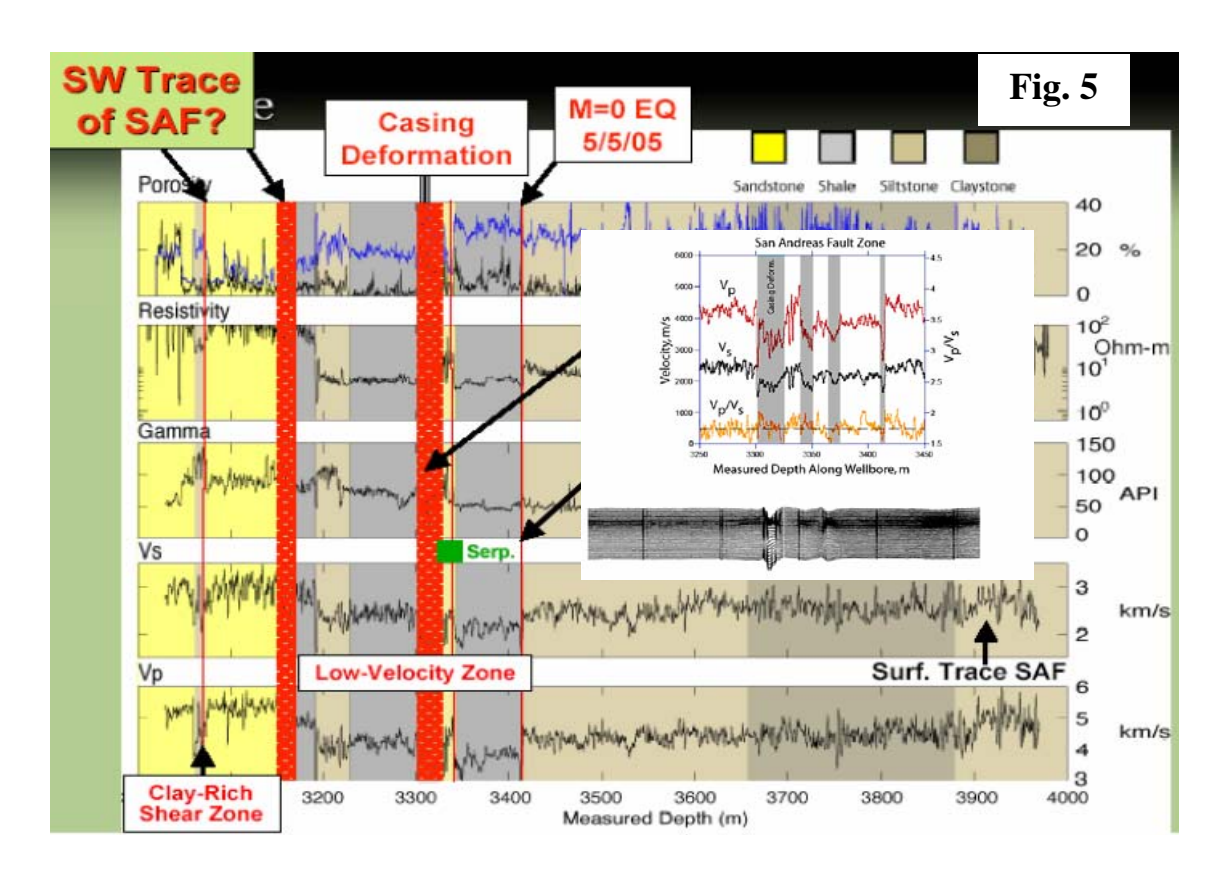
hole (≤28°) appears to be a typical feature of a weak fault embedded in a strong crust and a weak upper mantle with laterally variable heat flow. The predicted stress magnitudes indicate low shear stress on planes parallel to the fault but a very anomalous mean stress, approximately twice the lithostatic stress.

Chery et al. (2004) conclude that in central California, the rotation in the maximum shear stress orientation from very high angles of > 80° to the SAF in the far field to near field ~63° at 2 km depth in the pilot hole is also compatible with stress orientation deduced from earthquakes near the SAF in southern California. This would precludes the large stress rotations of ~45°in the vicinity of the SAF predicted by strong SAF/strong crust models such as that of Scholz (2000). Apart from stress rotations the model also predicts that the magnitude of the minimum principal stress in the core of the SAF is about two times lithostatic.

#### 6. Evidence of deformation in SAFOD drill hole

Deformation in SAFOD drill string casing (Fig. 5a and 5b) detected at depths of 3310-3353m suggested that displacement could occur over the short-term simultaneously along several closely correlated zones of brittle shear localization (Zoback et al. 2005). Fig. 5 shows potential shear zones indicated by anomalous geophysical properties, drilling rate, changes in cuttings mineralogy or increases in mud gas content are located at 3.19, 3.33, and 3.41 km MD (Hickman 2005). The anomalous zone at 3.33 km is particularly interesting, in that it is a 13-m-wide zone associated with the sudden appearance of serpentinite, which is seen along surface exposures of the SAF in central California and is thought to be important in controlling frictional strength and the stability of sliding. Which of these zones are currently active will be determined through repeat logging of SAFOD to identify further casing shear and locating the SAFOD target earthquakes with seismic instruments placed directly within the fault zone at seismogenic depths.

**Fig. 5.** Drilling logs and SAF shear zones. The shear zones are marked by sharp changes in different geophysical signals. Inset shows a highly exaggerated representation of casing shear due to creep on more than one slip surface (After Tembe et al. 2005, Zoback et al 2005).



#### 7. Studies of ores, cuttings and fluids

Lockner et al. (2005) quantified the mechanical integrity of fault damage zones, by comparing crack densities grouped by crack length (0.046 to 10 mm) in granodiorites from the SAFOD pilot hole (2200 m depth) and the Nojima fault, Japan (1279 m depth). For both the SAFOD and Nojima boreholes only cracks of length>0.2 mm had high enough densities (20-40%) to result in strong crack interactions leading to mechanical weakening. This suggested that the damage zone in both fault zones were in a state of structural failure for scales larger than the grain size, and essentially had lost cohesion. Both samples showed evidence of repeated episodes of fracture and hydrothermal healing. However, to the naked eye the studied samples appeared as 'typical' granodiorite, with no evidence of permanent shearing. Lockner et al. (2005) interpreted these properties as resulting from periodic passage of high amplitude dynamic stress waves associated with earthquake rupture.

Almeida et al. (2005) reported progressive increase in fractures in the siltstone toward the core of the fault located at 3067.2m (slickenside surfaces). The fault core at this location contained sheared gouge layers and slivers of very fine sandstone. This fault located specifically at 3064.7 to 3067.2m was thought to be the largest-displacement fault zone found in the spot cores of the phase 2.

Schleicher et al. (2005) reported on a number of mudrock drill cuttings from shear zones at 1500m and 3066m depths showing abundant polished surfaces with occasional slip striations. Electron microscopy (SEM, TEM) and X-ray mineralogy revealed the occurrence of thin clay film coatings containing smectite, chlorite, illite, quartz, albite and a possible serpentine mineral. The coatings were distinct from drilling mud montmorillonite by their higher Fe, Mg and K content and a lower Si-Al ratio. They suggest that these well-oriented smectite coatings are partly precipitated from percolating solutions during fault creep.

van der Pluijm et al. (2005) reported on preliminary observations of phyllosilicates in cuttings, including mineralogical and elemental data (XRD and ICP), and electron beam (SEM and TEM) characterization of mineralized surface polishes in fault horizons. It is noted that there are some significant problems with the use of cuttings for the study of phyllosilicates in the retrieved drilling material (e.g. mixing of cuttings as they travel from the drill face to the surface, "dilution" of phyllosilicate signatures from shear and alteration zones that are thinner than the 10 ft sampling interval, and possible contamination from montmorillonite in the bentonite drill mud). As shown in studies of exhumed faults, the SAFOD Pilot Hole revealed multiple populations of phyllosilicates, including mixed-layer clays in the shallow sedimentary rocks and chlorite in deeper granitic rocks. These findings indicate that there are variations in phyllosilicate mineralization with (1) depth (2) strain energy, deformation mechanism, and position in fault zone and (3) time. There are several zones of phyllosilicates in the SAFOD Main Hole, including: (1) a zone at 7800-8100 ft MD, marked by an increase in the amount of illite, and the appearance of a mixed-layer illite-smectite (I-S) phase; (2) a zone at 8400-8800 ft MD that includes at least one large shear zone marking a large increase in the amount of I-S and illite relative to surrounding protolith; (3) a zone at 11050-12400 ft MD marked by a large increase in the amount of chlorite that is fairly constant to the bottom of the hole, and the appearance of a mixed-layer clay.

Kirschner et al. (2005) analyzed the major and minor element chemistry and

stable isotope composition of samples from 3 sections of the SAFOD drill hole in order to document fluid-rock interactions in the San Andreas and associated fault zones. The elemental chemistry of samples from 10450 to10530 ft MD interval does not vary significantly. Only Mg, Yt, and Ba increase and Ca decreases moderately downhole across this interval. The Yt and Ba variability is potentially due to variable contamination of barite-bearing mud in the cuttings. In samples from 10860 to 11000 ft, Fe, Mg, and K increase and Ca decreases moderately downhole. In sample interval 11400 to 11540 ft, Fe increases and Ca decreases slightly downhole. The other major and minor elements in the XRF analyses do not vary much across these three intervals. These variations in elemental chemistry correspond to mineralogy changes across these intervals. Carbon and oxygen isotope values of carbonate veins and breccias from the 10450 and 11400 ft intervals range from 0 to +8 per mil (carbon) and 14 to 20 per mil (oxygen), consistent with carbonate precipitation from fluids that had isotopically exchanged with silicates.

Petrological and microstructural analyses of drill cuttings were conducted by Barton et al. (2005) on SAFOD PH and MH at 100 ft intervals collected from the PH to a depth of 2164 m (7100 ft) and from Phase 1 to a depth of 3067 m (10062 ft). Lithologic features in the Quaternary/Tertiary deposits from 30-640 m (100-2100 ft) in the PH, and 670 - 792 m (2200 - 2600 ft) in the Phase 1 MH, include fine-grained, thinly bedded sediments with clasts of fine-grained volcanic groundmass. Preliminary grain mounts analysis from 1920-3067 m (6300 - 10062) in the Phase 1 main hole, indicates a sedimentary sequence consisting of fine-grained lithic fragments of very fine-grained shale. Deformation mechanisms observed within the cuttings of granitic rocks from 914 -1860 m (3000 - 6100 ft) include intracrystalline plasticity and cataclasis. Intracrystalline plastic deformation within quartz and feldspar grains is indicated by undulatory extinction, ribbon grains, chessboard patterns, and deformation twins and lamellae. Cataclastic deformation is characterized by intra- and intergranular microfractures, angular grains, gouge zones, iron oxide banding, and comminution. Shear zone (identified based on wt.% cataclastic grains of the cuttings) occurred at 1150-1420 m (3773 - 4659 ft.) depths in the PH, and are consistent with locations recognized by Boness and Zoback (2004) as shear zones using borehole geophysical data. These shear zones may possibly be correlated to shear zones identified in the Phase 1 main hole from 1615 - 2012 m (5300 – 6600ft). If this is the case, it can be explained by steeply dipping subsidiary fault zones, likely associated with the SAF.

Downhole fluid samples from both the SAFOD pilot hole (1443-1470 m) and the SAFOD main hole (2540-2557m) were studied by Thordsen et al. (2005). Chemical data showed that these samples are a mixture of Formation water (75-80%) and the dyetagged drilling solution. High pH values (9.5-10.5) and high Ca concentrations indicate contamination from the cement used for casing the well. Results show a Na-Ca-Cl type water with a salinity of ~20,000 mg/L TDS, very low Mg (0.1 mg/L) and carbonate alkalinity (<1 mg/L). This chemical composition is typical of formation water from sedimentary rocks, such as oil field waters from California. The deepest samples from SAFOD main well are extremely gas-rich, with calculated in-situ gas pressures exceeding 50 bars. Low O2 (<0.02%) and high N2/Ar ratios reveal a strong non-atmospheric N2 component. Helium was enriched by a factor of ~1500X over the level in air-saturated water, and 3He/4He ratios yielded R/Ra values of 0.33 to 0.36, indicating a small mantle He contribution to the fluids. Although the near absence of CO2 (<0.002%) may be an

artifact of high pH, the relatively low R/Ra values compared to the nearby Varian-Phillips well (CO2 ~40% of total gas, R/Ra=1.5) and other wells in the Parkfield area indicate a relatively low flux of CO2 and other mantle volatiles, and a relatively minor contribution of these fluids to the San Andreas system at the SAFOD location and depth.

Solum et al. (2005) correlated XRD peaks of cuttings and core samples to well log data in order to establish a clay mineral assemblage signature for the deformed and undeformed (protolith) SAFOD rocks (Fig. 6). The method identified two zones of laumontite (zeolite) mineralization, one in the granodiorite at ~244-1923 m (800 to 6310 ft), and one in a deeper arkose at ~2682 to 3158 m (~8800 to 10,360 ft). Trace amounts of laumontite were associated with a possible shear zone at ~3338 m (10,950 ft), but no clear relation between zeolite mineralization and other shear zones penetrated by SAFOD has been observed. The main hole entered a sequence of shale/siltstone/fine sandstones at ~3158 m (10360 ft) MD, indicating the presence of a significant fault. Below this depth the chlorite (001) XRD peak widths exhibited little variability (~0.35-0.4 compared to a broad range of  $\sim 0.15$ -0.6 above that depth, indicating a major change in lithology). There is also a very pronounced change in the clay mineral assemblage at ~3353 m (11000 ft) MD, below which clays (chlorite, illite, and a possible mixed-layer phase) exhibit little variation both in abundance and crystallinity, indicating the presence of a significant fault at approximately that depth (Fig. 7). This is broadly consistent with the first appearance of serpentinite minerals at ~3322 m (10900 ft) MD, and a sudden increase in the

**Fig. 6.** Preliminary XRD mineral assemblage identification of some shear zones encountered in SAFOD (Solum et al. 2005)

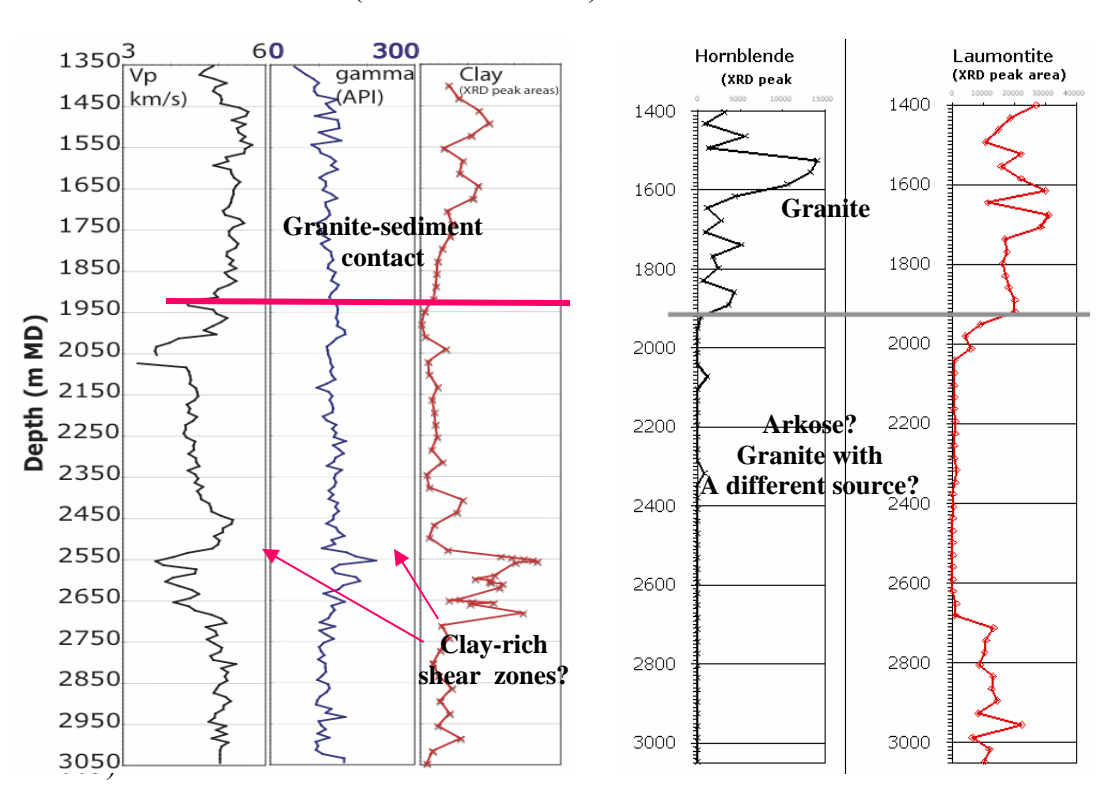
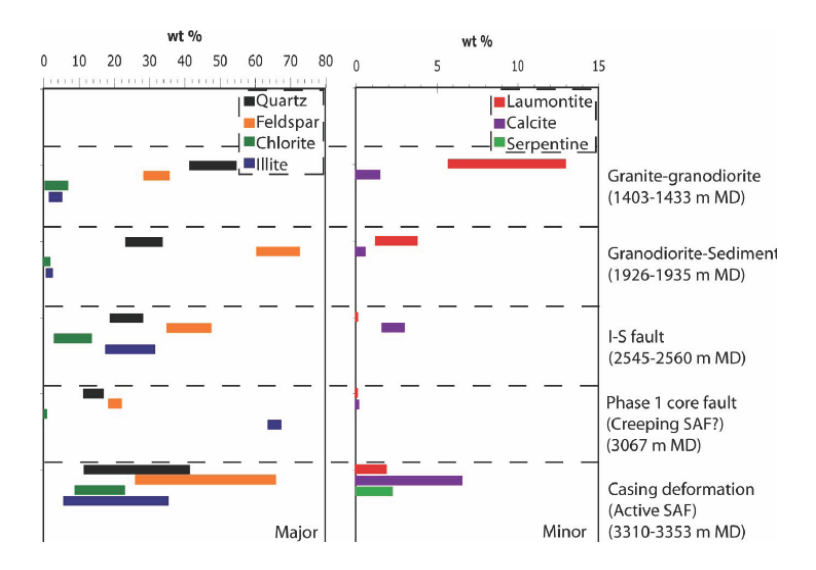


**Fig. 7.** A comparison between changes in the composition of protolith (left ) and deformation-related clay minerals with depth in the SAFOD MH (Solum et al. 2005)



concentration of methane dissolved in the drilling mud at 3338-3344 m (10950-10970 ft). As shown in Fig. 7 a mixed-layer illite-smectite phase is present in a major fault zone at ~2554 m (8380 ft). This phase is present both in bulk cuttings as well as in plucked grains of fault rocks, indicating that it is not a contaminant from the drilling fluid. A minor illite-rich mixed-layer illite-smectite phase is also present in a clay-rich shear zone at ~3067 m (10,062 ft) MD, sampled during a coring run in 2004. The restricted occurrence of these phases in and adjacent to shear zones suggests that they are syn-deformational, fault-related phases. The generally low coefficient of friction of smectites suggests that the formation of these phases may weaken the fault zone. Elevated smectite content in clay mineral composition of shear zones has been reported (Fig. 8) in other fault drilling projects.

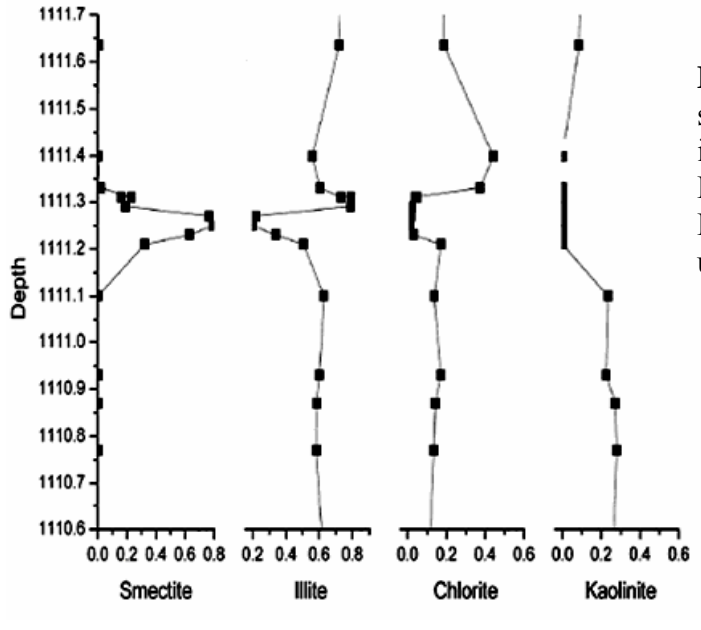


**Fig. 8.** Clay content in a shear zone encountered in Taiwan Chelungpu Drilling Project (TCDP) Hole A (Kuo and Song unpublished).

(10,062 ft) MD, sampled during a coring run in 2004. The restricted occurrence of these phases in and adjacent to shear zones suggests that they are syn-deformational, fault-related phases. The generally low coefficient of friction of smectites suggests that the formation of these phases may weaken the fault zone. Elevated smectite content in clay mineral composition of shear zones has been reported (Fig. 8) in other fault drilling projects.

Two shear zones are enriched in iron oxides, one at 1923 m (6310 ft) MD, where the hole leaves granodiorite and enters sedimentary rocks, and one at 3158 m (10360 ft) MD, where the hole leaves a series of arkoses and enters a sequence of siltier rocks. The absence of iron oxides in other fault zones sampled by SAFOD indicates that the fluid-rock interactions in these two fault zones were different from the rest of the SAF system at this location.

#### 8. Friction studies

Arguments for a weak SAF, based on surface heat flow and stress orientations suggest coseismic frictional strength of 0.1 to 0.2. Tembe et al. (2006) conducted laboratory tests on SAFOD cuttings and core samples from 2300 to 3100m MD. The samples were crushed and sieved to obtain particle sizes of <149  $\mu m$  for 30° sawcut friction experiments with 1 mm-thick gouge layers at constant effective normal stresses of 10 and 40 MPa and constant pore pressure of 1 MPa. Samples were sheared up to 10.4 mm at room temperature and velocities of 1, 0.1 and 0.01  $\mu m/s$ . Stable sliding behavior and overall strain hardening were observed in all tests.

Preliminary results yield coefficients of friction, which generally fall into two clusters spanning the range of 0.45 to 0.8 (Figs. 9a-b). The higher values 0.7 – 0.8 correspond to quartzo-feldspatic samples derived from granodiorite and arkoses encountered in the drill hole, comparable to frictional strength of 0.68 measured during sliding on faults formed in fracture tests of intact SAFOD granodiorite samples. Sliding tests were also conducted on core samples obtained from a narrow prominent fault zone at 3067 m measured depth. Coefficient of friction was measured to be 0.40-0.45, and was notably weaker than that for cuttings (0.6) tested at this same depth but similar to the values obtained for other shear zones (Fig. 10). The lower friction values correlated with depth intervals interpreted to be broad shear zones based on enriched clay content, reduced seismic velocities and increased gamma radiation. Chen et al. (2005) compared Nankai drill site 297 mudstone friction results with clay-quartz mixture simulated gouge experiments in which friction dropped to about 0.1-0.2 with increasing illite/smectite content of the simulated gouge. However, the friction tended to increase for some types of clay gouges (e.g. montmorillonite, talc, and graphite) with increasing normal stress.

Overall, the study by Tembe et al (2006) suggests frictional strengths of some SAF rocks at SAFOD exceed 0.4 (Fig. 11). The study concludes that if SAF is unusually weak, the presence of alteration minerals appears to account for only a portion of this reduced strength and other mechanisms such as elevated pore fluid and dynamic weakening processes would still be required. Combined XRD (Solum 2005) and friction results (Tembe et al. 2006) for the SAFOD cuttings and core samples is shown in Fig. 12.

Saffer and Marone (2003) showed in simulated gouge that smectite clays tend to velocity strengthen with increased normal stress. The transition occurred from velocity weakening to velocity strengthening behavior at about 30-40 MPa. Experiments with

serpentinite (antigorite, chrysotile) at 25MPa normal stress (Reinen et al. 1998) suggested that at high sliding speeds (1-32  $\mu$ m/s) the material tends to be velocity weakening while at slower sliding rates (0.0005-0.1  $\mu$ m/s) it showed a velocity strengthening behavior. The velocity dependence data compiled by Paterson and Wong (2005) for different material and conditions is shown in Fig. 12.

**Fig. 9.** Friction experiment results. (a) Cuttings 2560, 2377-2713 sample depths (b) Cuttings from NE side of the SAF at 3991m sample depth. Similar results were obtained for core samples (Tembe et al. 2006)

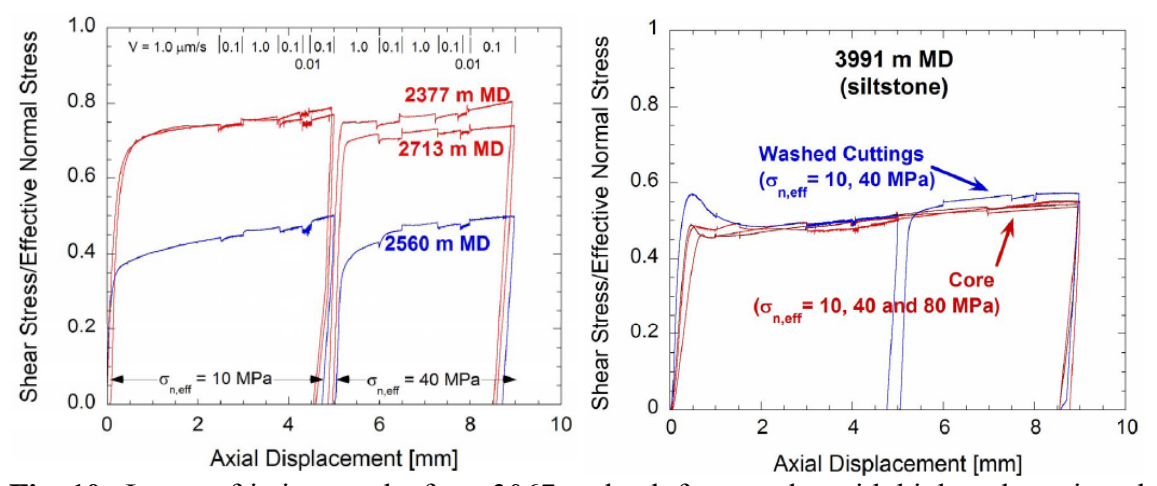


**Fig. 10.** Lowest friction results from 3067 m depth for samples with higher clay mineral content (Tembe et al. 2006)

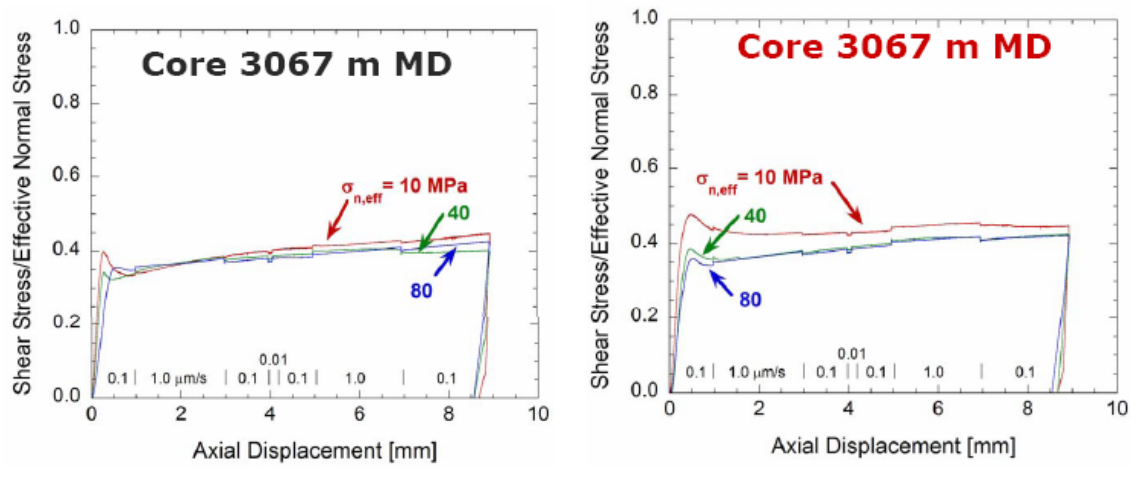
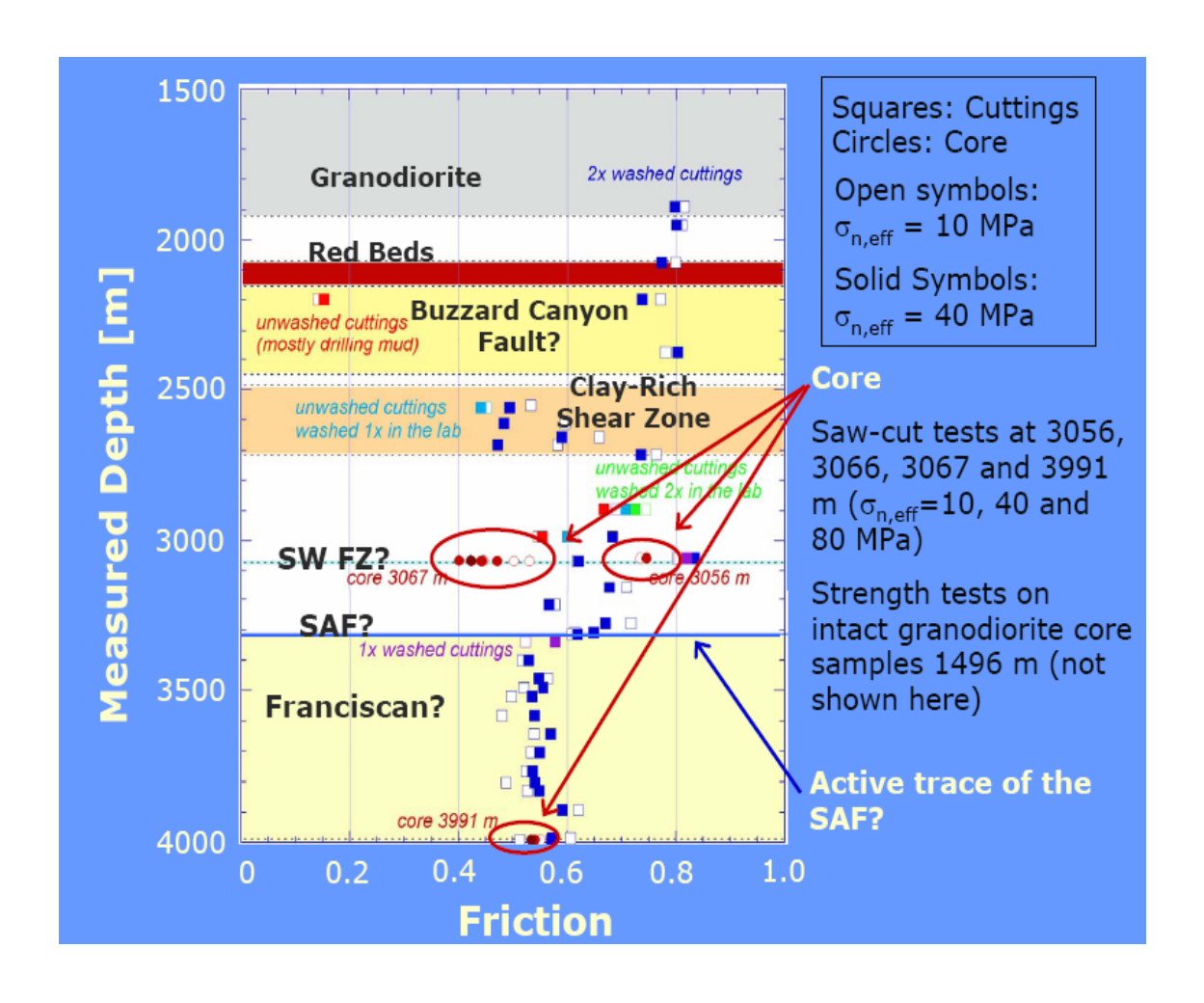
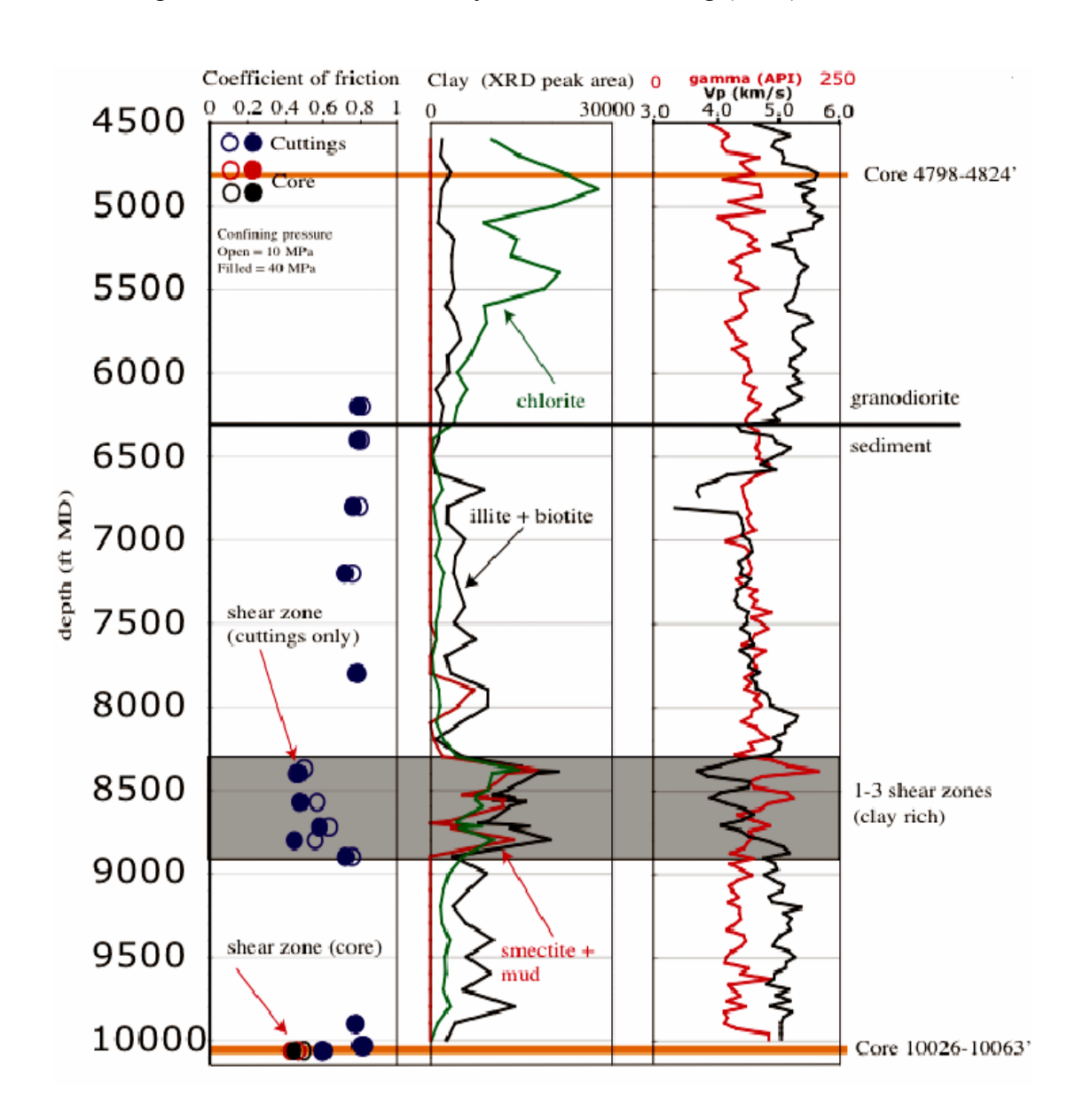


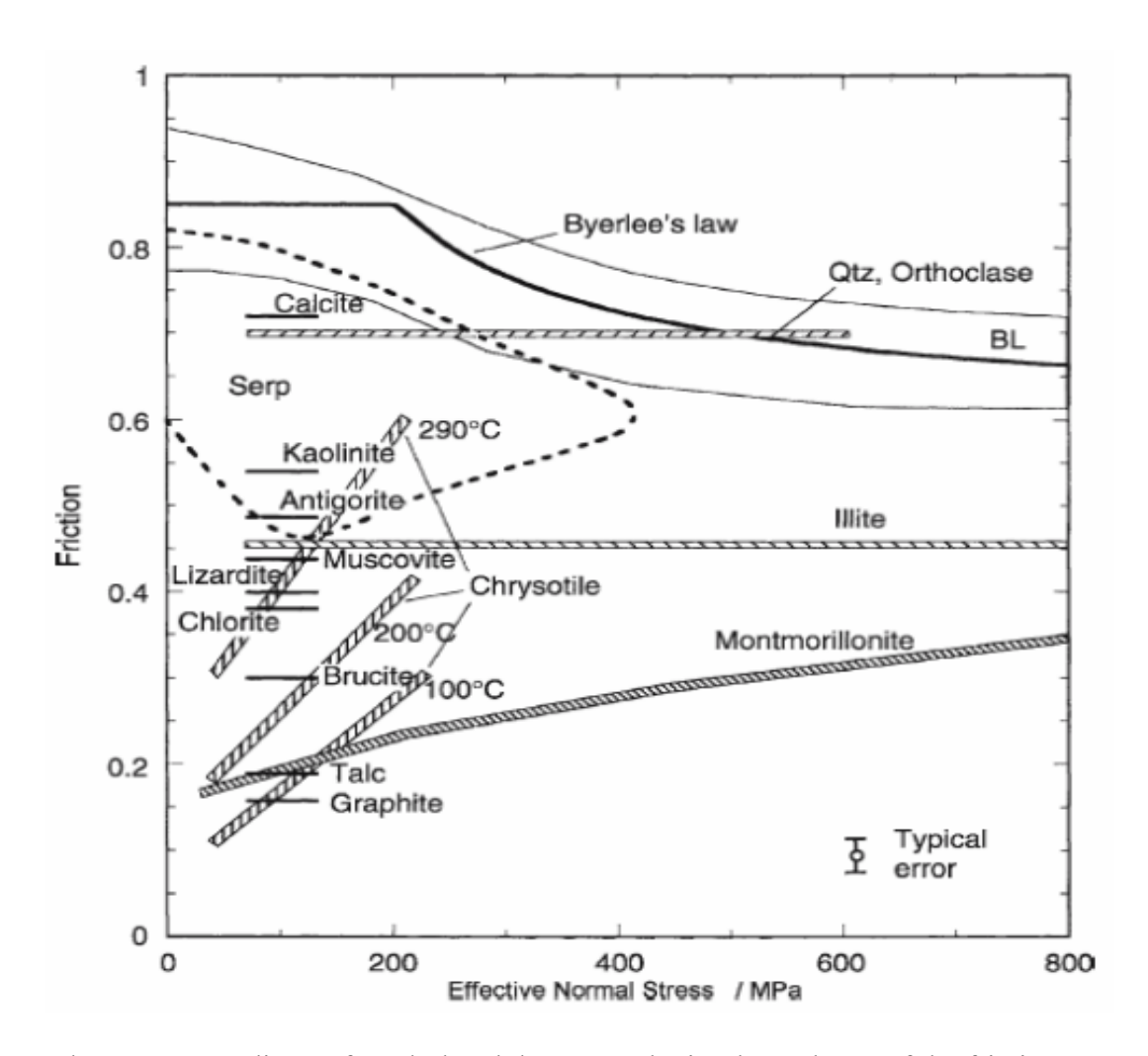
Fig. 11. Friction data for all experiments vs. depth of drilling (Tembe et al. 2006).



**Fig. 12.** Experimental friction data for clayey and non-clayey gouges vs. Byerlee friction law, compiled from various studies by Paterson and Wong (2005)



**Fig. 13.** Experimental friction data for clayey and non-clayey gouges vs. Byerlee friction law, compiled from various studies by Paterson and Wong (2005)



Also see Appendix A4 for tabulated data on velocity dependence of the friction coefficient for steady-state sliding at room temperature from different experimental studies.

## 9. Samples and sections of set 1, Hadizadeh et al. 2006

### 9a. summary table of the samples and thin sections

Depth ft, inch Box Phase Thin Section(s)

4000 5	•						
4800, 5	2	1	P1A, P1B				
• 4802, 0	1-2 inch SZ, dipping SE, mantled by alterations and a bordering fracture zone.						
• 4805, 5.6	1-2 inch SZ with some alterations.						
4806, 0	3	1	2A1, 2A2, 2B1, 2B2, 2bottom				
10037, 0	14	1	3A1, 3A2				
• 10037, 2.7	1-1.5 inch SZ and fractures						
10044, 8 to 10044, 10	16	1	4A1 (br. 4A1), 4A2, 4B1, 4B2				
10045, 4.5 to 10045, 6.5	16	1	5A1, 5A2, 5A3, 5B1, 5B2 (br. 5B2), 5B3	2			
• 10045, 9.7	Small variable thickness, shallow-dipping SZ with fracture zone either sides.						
10046, 3	17	1	P2A, P2B				
• 10047, 8.25	2 inch thick, shallow dipping SZ separating coarse Sst. (top), and very fine Sst.						
10048, 8	17	1	P3				
13091, 6	1	2	P4				
13095, 4	2	2	P5	3			
13100, 8	3	2	P6				

Brackets 1, 2, and 3: see 9b; Depths are measured depths (MD); br.= broken slide.

Phase 1: 0 to 3700ft and 3300 to 10060ft

Phase 2: 10065 to13082ft

9b. general lithological description of the sampled spot cores (Almeida et al. 2005, Chester et al. 2005)

- 1. 4798 to 4824ft (1476-1484m) cored interval in phase I consists of a medium-grained hornblende-biotite granodiorite with leucocratic phynocrysts and lenses that are weakly foliated in some places. Small shears, fractures, and veins that record both high- and-low temperature shear deformation are present in this cored interval. The dominant brittle deformation features are series of subvertical fractures and moderate dipping shears, both of which contain some secondary mineral fill and display centimeter(s)-thick halos of low-grade alteration and staining of the granodiorite host.
- 2. 10025' to 10063' (3085-3096m) cored interval in phase I composed of pebble conglomerate to coarse-grained arkosic sandstone with lithic fragments of granite, sandstone, siltstone, and volcanic clasts. The beds are massive, well-cemented and contain rare cobble-sized clasts. The lower section is a fine-grained, well-cemented arkosic sandstone that grades downhole into a fine-grained siltstone. Bedding is indistinct throughout this section. This interval is crosscut by numerous fracture sets that record multiple stages of deformation and fluid infiltration. The dominant brittle features include irregular, somewhat diffuse cataclastic bands, up to two centimeters thick, that are oriented at high angles to the core axis, and thinner, dark colored shear fractures that are up to several mm thick. Shear fractures are common in the pebble conglomerate and very coarse sandstone, and display consistent kinematic indicators and preferred orientations. Two minor faults are present in this depth interval. On the basis of juxtaposition of different rock types, these faults likely have displacements of at least several meters.

Draper et al. (2005) presented two possible cases that have shallow sedimentary sequence similar to sedimentary sequence of the SAFOD phase 1 drilling (6305 ft to 10360 ft): the Eocene Butano (or equivalent Point of Rocks Sandstone) or the Miocene Vaqueros (or equivalent Temblor Formation). These formations were both deposited as deep sea fans from a Salinian basement source and were significantly more conductive and less fractured than the granite and granodiorite above, although both units display similar seismic velocities. Core and cuttings samples show that the rocks are arkosic, grading from conglomerates to shales/mudstones. Clasts are generally angular to subangular, indicating a texturally immature sedimentary sequence. Point counts show a dearth of volcanic grains with abundant granitic clasts, indicating granitic provenance.

Evans et al. (2005) examined thin sections of grain mounts and loose, washed grains from cuttings from 10,100 to 12,900 feet measured depths (md), and used X-ray diffraction analyses to determine rock types in the deeper part of the borehole. The most significant lithologic change occurs at 10,300 to 10,700 ft md, where the dominant rock type changes from arkosic sandstone and shale above to dark green and grey siltstone and shale below. Locally in the lower section there are zones of sheared siltstone and shale. The lithologic transition is nearly complete by 10,800 ft md. Serpentine grains are evident starting at approximately 10,900 ft, some with mesh texture (pseudomorphic after olivine), and some pseudomorphic after pyroxenes. Minor amounts of serpentine are found at the 10,970 to 11,000 ft interval, which is associated with an increase in gas in the borehole. At depths >11,000 ft md, shale and siltstone fragments containing quartz, plagioclase, biotite, and K-feldspar are common, and calcite is abundant, occurring both as separate grains and as veins, cement, and alteration minerals in other rock fragments. Fossil fragments (Inoceramus) are observed in several of the samples, indicating a minimum Cretaceous age for these rocks. At some intervals the washed cuttings have 10

to 30 % green, sheared, lozenge-shaped grains of phyllosilicate-rich rock. Deeper in the hole (11,500 to 12,500 ft) some grains exhibit sheared phyllosilicate surfaces, and some sandstone fragments contain plagioclase, biotite, and K-feldspar. Serpentine grains are found at 12,700 to 12,900 ft md, along with shale and siltstone fragments.

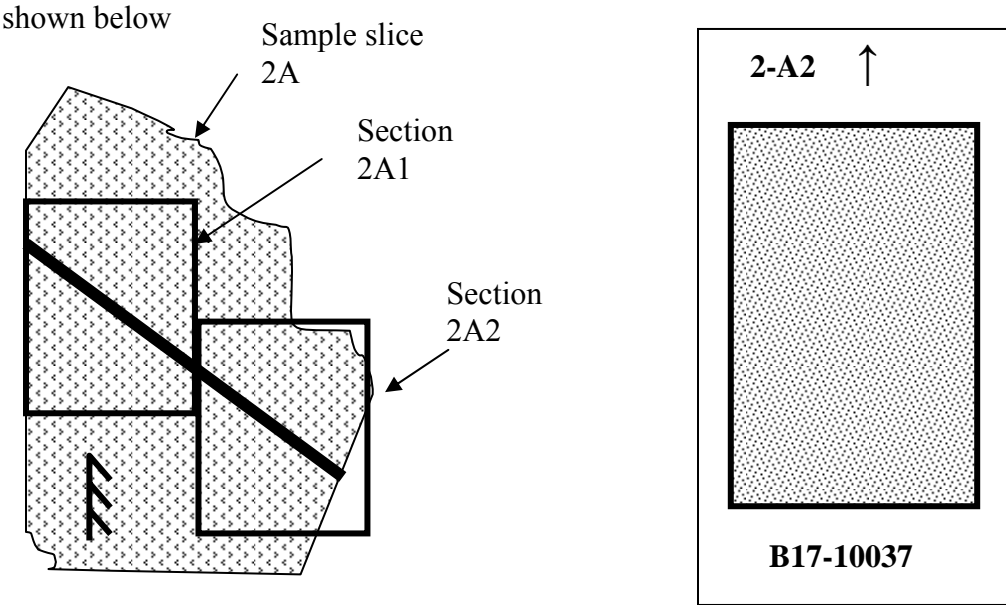
3. 13090 to 13116' (4028-4036m) cored interval in phase II consists of shale with a few beds of siltstone and very fine-grained Sst. Graded bedding, fossil fragments, and bioturbated sections are present. Deformation features include numerous small veins, scaly fabric, and some polished slip surfaces.

A total of 60m Spot core were taken during Phases 1 and 2 as follows.

- 20 m of 4" diameter core in 2004 (26 ft at 1.5 km, 38 ft at 2.5 km)
- 40 m of 4" core in 2005 (4 cores between 2.5 and 3.2 km)

#### 9c. thin section numbering and labeling format

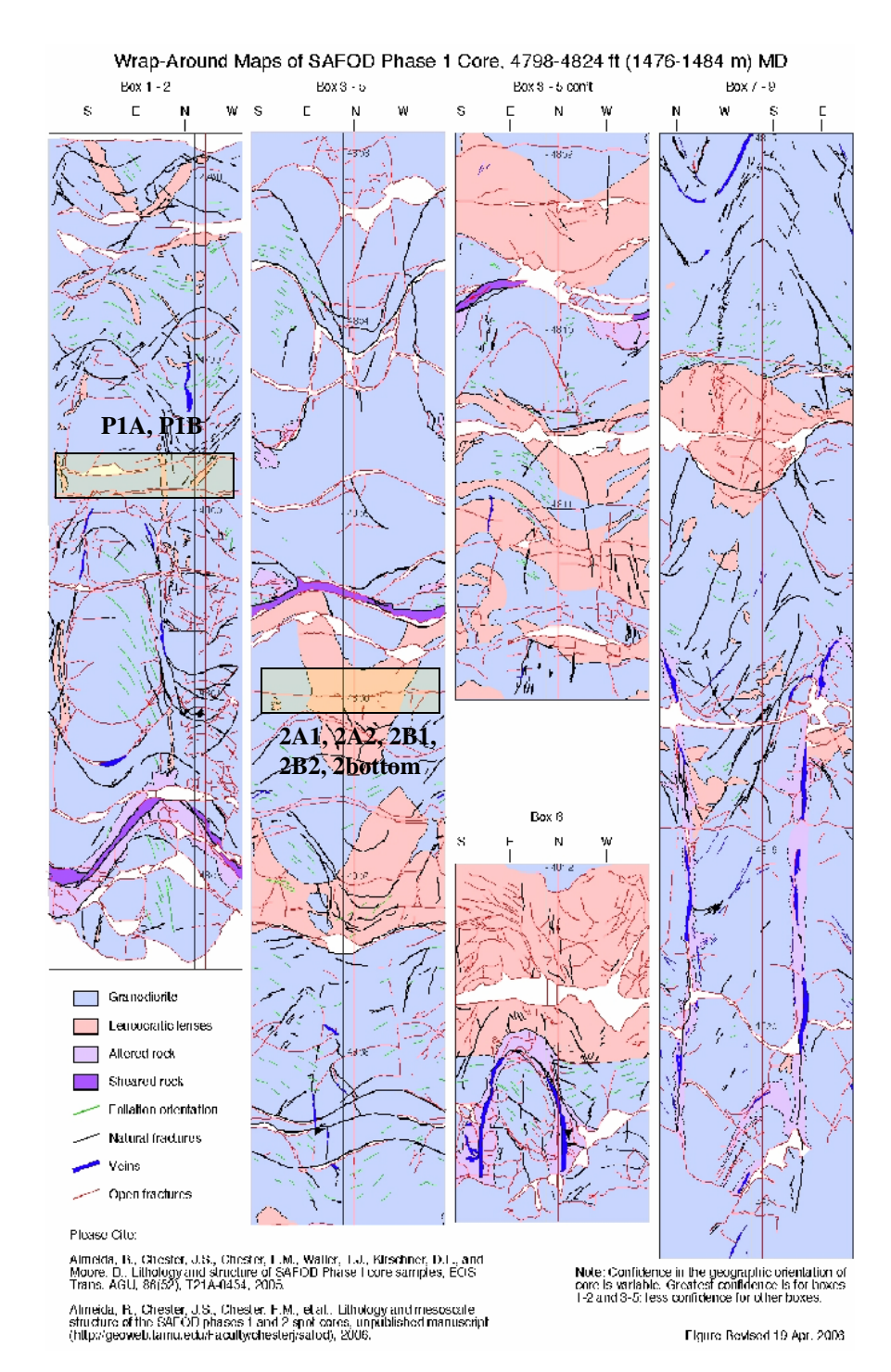
Protolith sections are designated P1 through P6 with A and B subs. Sections that include shear zones and fractures are numbered 2 through 5 with A and B subs and their numbered subs 1...n. e.g. 2A1, 2A2, 2A3 and so on. In each case the order is from top to bottom (determined from the top arrow on the samples), so 2A1 is the section located above 2A2 in a slice from the sampled core. The general form for covering a slice is

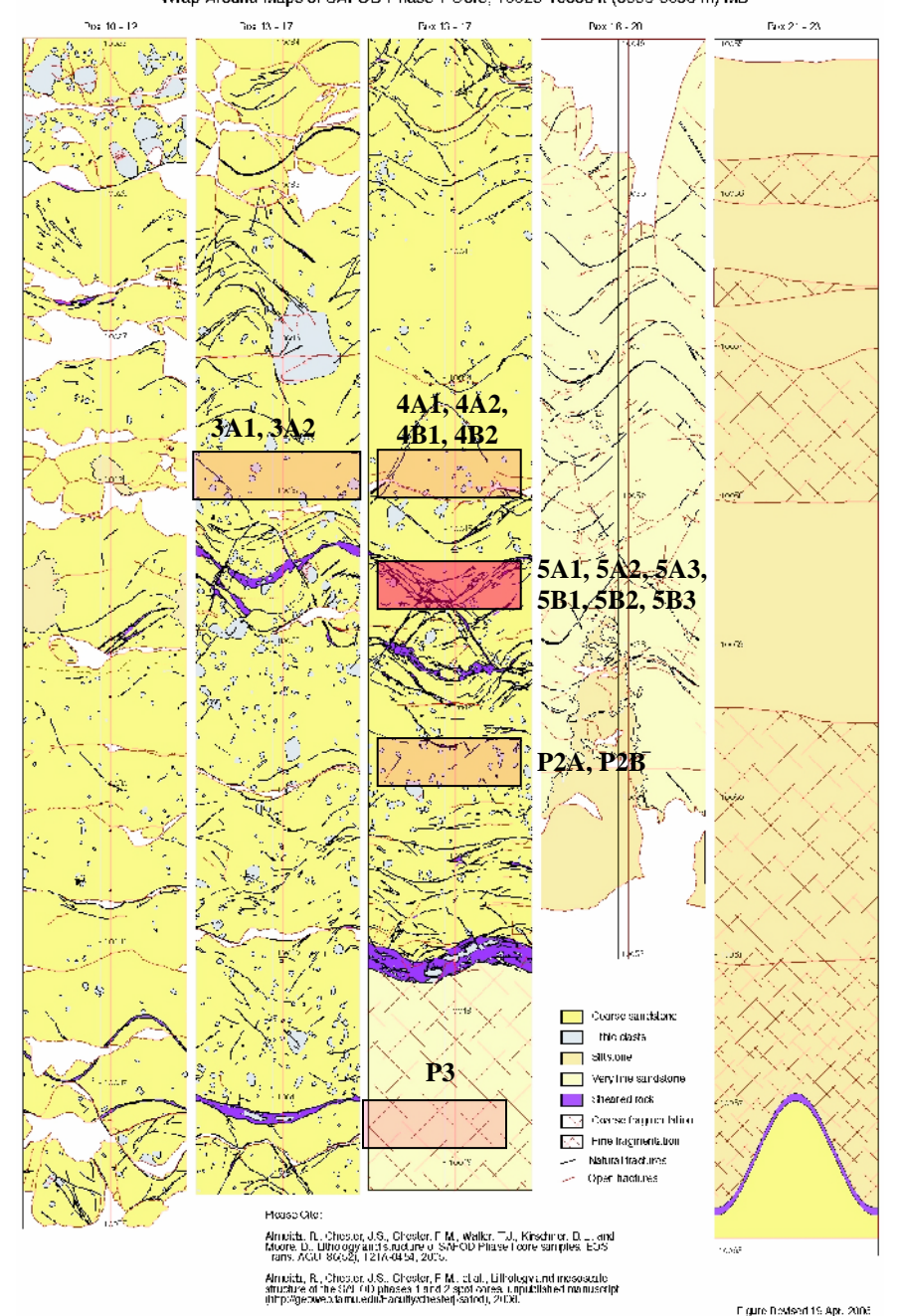


#### Thin section labels

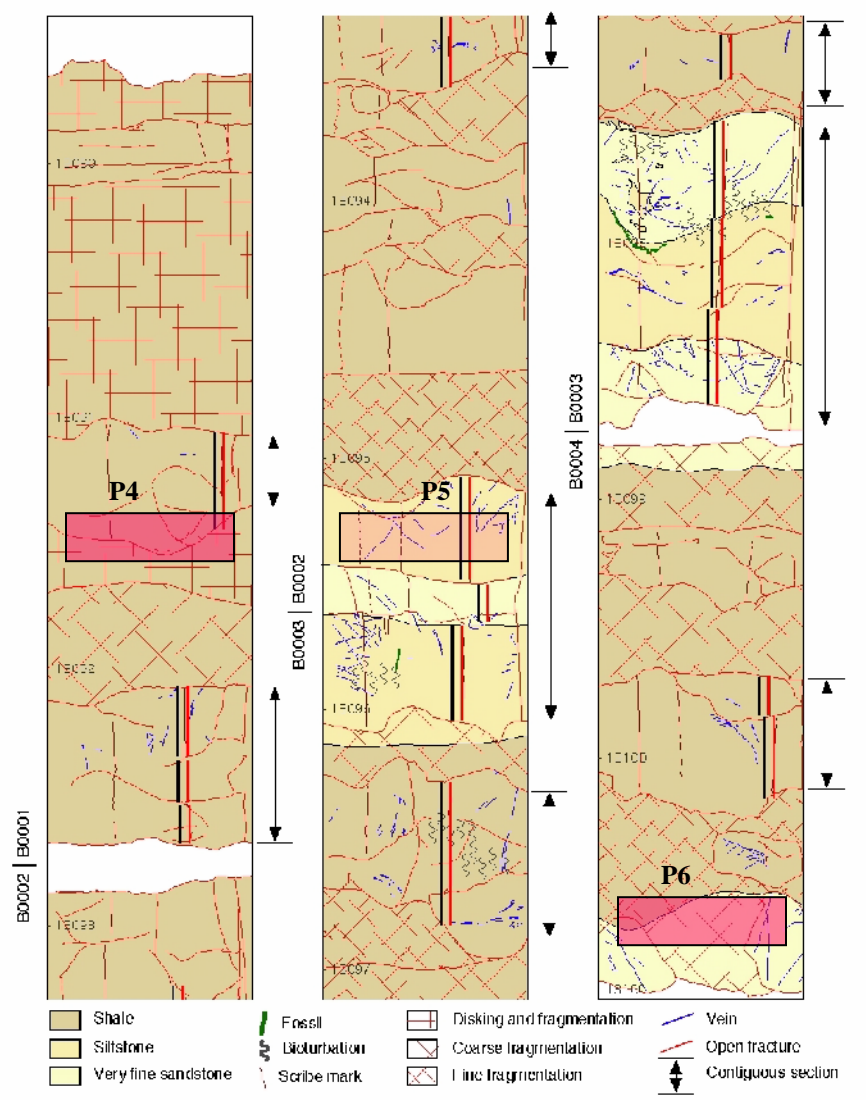
Top: section number and top arrow Bottom: box number followed by the depth in ft

# Map Key Granodiorite Leucocratic lenses Altered rock Sheared rock Shale Siltstone Very fine sandstone Coarse sandstone Lithic clasts Foliation orientation Natural fractures Veins Fossil Bioturbation Scribe mark Open fractures Disking and fragmentation Coarse fragmentation Fine fragmentation





#### Wrap-Around Maps of SAFOD Phase 2 Core, 13090-13116 ft (4028-4036 m) MD



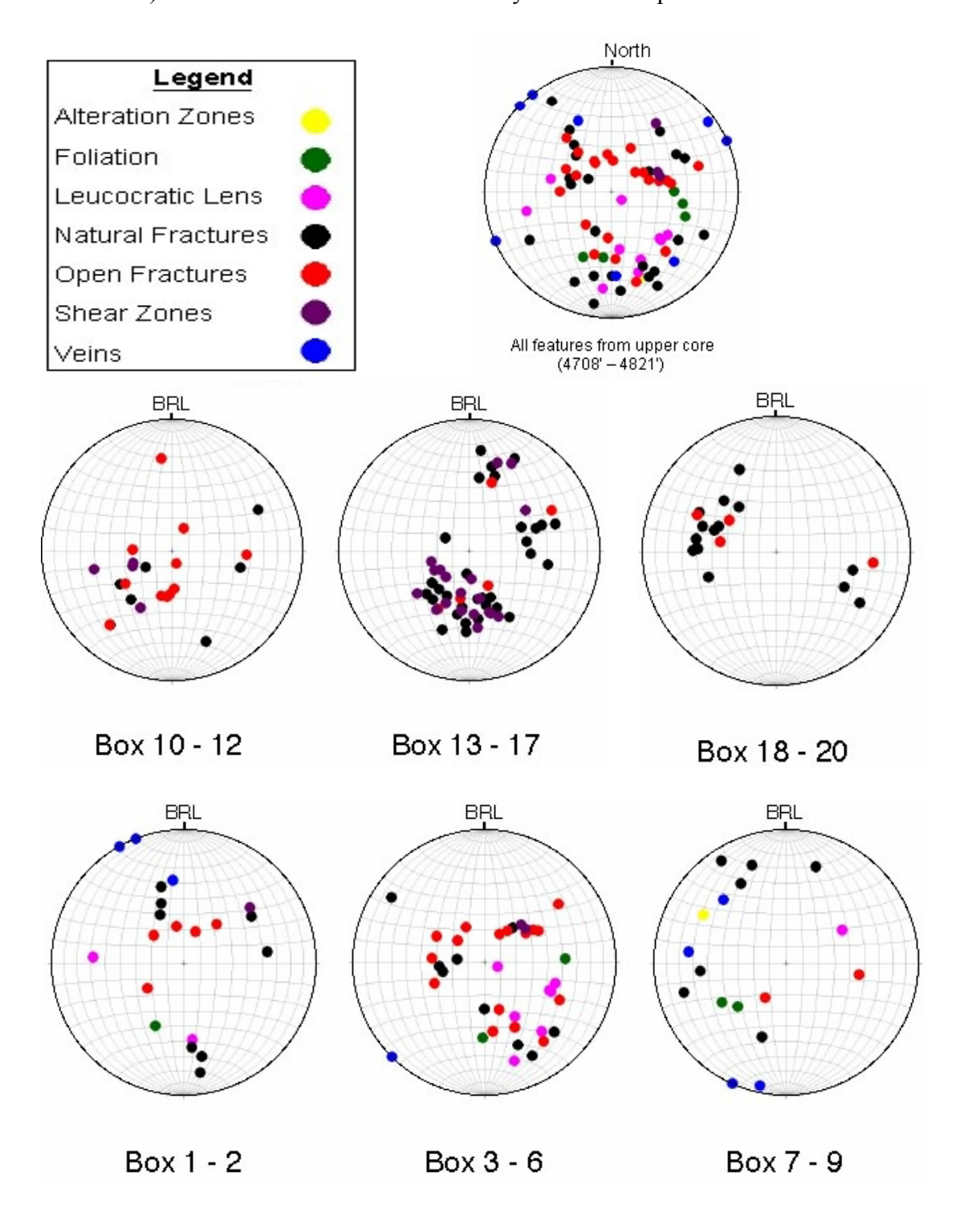
Please Cite:

Almelda, R., Chester, J.S., Chester, F.M., Waller, T.J., Kirschner, D.L., and Moore, D., Hilhology and structure of SAFOD Phase Lorie samples, EOS Trans. AGU, 86(52), 121A-0454, 2005.

Almelda, T., Chester, J.S., Chester, T.M., et al., Ellindogy and mesoscale structure of the SALOD phases 1 and 2 spot cores, unpublished manuscript (http://gooweb.tarmi.edu/Faculty/chester/&afod), 2006. Ligure Revised 19 Apr. 2006

## 9e. equal area projection of the internal structures in the sampled cores

Lower hemisphere, equal area projections onto surface perpendicular to core axis relative to the core's black reference line (BRL) marked on core surfaces (After Almeida et al. 2005). For box numbers see the summary table of samples and thin sections.



#### REFERENCES

- Almeida R., Chester J., Chester F., Kirschner D., Waller T., Moore D. Mesoscale Structure and Lithology of the SAFOD Phase I and II Core Samples. AGU Abstr., T21A-0454, 2005.
- Barton D. C., Solum, J.G., Evans J. P. Structural and Lithologic Characterization of the SAFOD Pilot Hole and Phase One Main Hole. AGU Abstr., T21A-0451, 2005.
- Boness N. L., Zoback M. D. Stress-induced seismic velocity anisotropy and physical properties in the SAFOD pilot hole in Parkfield, CA. GRL 31, in press.
- Chen N., Louis L., Tembe S., Wong T-F., Lockner D., Morrow C., Li-Wei Kuo S.-R., David C., Robison, P. D., Zhu W. Taiwan Chelungpu-fault Drilling Project (TCDP). CIG Wksp., 2006.
- Chery J., Zoback M. D., Hickman S. A mechanical model of the San Andreas fault and SAFOD Pilot Hole stress measurements. GRL, 31, L15S13, doi:10.1029, 2004.
- Chester J., Kitajima H., Chester F., Shimamoto T. Dynamic Weakening of Ultracataclasite During Rotary Shear at Seismic Slip Rates. AGU Abstr, T21B-0472, 2005.
- Darcy K., McPhee R. C., J., Wentworth C. M., Crustal structure across the San Andreas Fault at the SAFOD site from potential field and geologic studies. GRL 31, L12S03, doi:10.1029/2003GL019363, 2004.
- Draper, S. D., Boness N. L., Evans, J. Occurrence and significance of the Sedimentary Rocks in the SAFOD Borehole: Preliminary Analysis. AGU Abstr. T24B-02, 2005.
- Ellsworth, W., Hickman S., Zoback M., Davis E., Gee L., Huggins R., Krug R., Lippus C., Malin P., Neuhauser D., Paulsson B., Shalev E., Vajapeyam B., Weiland C., Zumberge M. Observing the San Andreas Fault at Depth. AGU Abstr., T24B-04, 2005.
- Evans J. P., Moore D. E., Kirschner D., Solum J. G. Lithologic Characterization of the Deep Portion of the SAFOD Drillhole. AGU Abstr., T21A-0450, 2005.
- Griscom A., Jachens R. C. Tectonic implications of gravity and magnetic models along east-west seismic profiles across the Great Valley near Coalinga, USGS. Prof. Papers, 1487, 1990.
- Hickman S.H., Zoback M. D., Ellsworth W. L. Structure and Composition of the San Andreas Fault Zone at Parkfield: Initial Results from SAFOD Phases 1 and 2., AGU Abstr. T23E, 2005.

- Kirschner D. L., Evans J., Chester J., Chester F., Solum J., Moore D. Elemental and stable isotope chemistry of cuttings and core samples from SAFOD drill hole. AGU Abstr., T21A-0452, 2005.
- Lockner D A, Morrow C, Moore D. Crack damage in core samples from the San Andreas and Nojima faults. AGU Abstr. T21A-0449, 2005.
- McPhee D. K., Jachens R. C., and Wentworth C. M., Crustal structure across the San Andreas Fault at the SAFOD site from potential field and geologic studies. GRL 31, L12S03, doi:10.1029, 2004.
- Miller M. S., Anderson M. L., Jachens R. C., Wentworth C. M. 3-D geophysical model of the upper crust at the proposed San Andreas Fault Observatory at Depth (SAFOD) site near Parkfield, CA, Eos Trans. AGU Abstr. T21C-16, 2000.
- Paterson, M.S. and Wong, T.-f., Experimental Rock Deformation The Brittle Field, 2nd Edition. Springer-Verlag, New York, 348 pp., 2005.
- Roecker, S., C. Thurber and D. McPhee, Joint inversion of gravity and arrival time data from Parkfield: New constraints on structure and hypocenter locations near the SAFOD drillsite, GRL 31, L12S04, doi:10.1029/2003GL019396, 2004.
- Rymer M. J., Catchings R. D., Thayer M., Arrowsmith J. R. Structure of the San Andreas Fault Zone and SAFOD Drill Site as Revealed by Surface Geologic Mapping and Seismic Profiling Near Parkfield, California. AGU Abstr., T11F-08, 2005.
- Saffer D.M. and Marone C. Comparison of smectite- and illite-rich gouge frictional properties: application to the up dip limit of the seismogenic zone along subduction megathrusts. Earth Plan. Sci. Lett., 215, 219-235, 2003.
- Schleicher A. M., Warr L. N., van der Pluijm B., The Clay Mineralogy of fracture coatings observed in mudrock cuttings from the SAFOD borehole. AGU Abstr. T21A, 2005.
- Scholz, C. H., Evidence for a strong San Andreas fault. Geology 28, 163-166, 2000.
- Solum J. G., Hickman S. H., Lockner D. A., Moore D. Mineralogy of the SAFOD Main Hole: Detailed characterization of fault and country rocks. AGU Abstr. T24B-01, Fall 2005.
- Simpson, R. W., Jachens R. C., Wentworth C. M. Average topography, isostatic residual gravity, and aeromagnetic maps of the Parkfield region, California. USGS Open File Rep. 89–13, 1988.

- Tembe S., Lockner D., Solum J., Morrow C., Wong T-f., Moore D. Strength of the San Andreas Fault Zone: Insight From SAFOD Cuttings and Core. AGU Abstr., T24B-03, 2005.
- Tembe S., Wong T-f., Lockner D., Moore D., Morrow C., Solum J., Chen N., Louis L., Song S-R, Kuo L-W., David C., Robion P., Zhu W. Fault Rheology: Constraints from laboratory measurements on core samples from deep drilling into fault zones. Joint Presentation of SAFOD and the Taiwan Chelungpu-fault Drilling Project (TCDP) at the CIG Workshop, 2006a.
- Tembe S., Lockner D., Solum J., Morrow C., Wong T.-f., Moore D. Implications for strength of the San Andreas Fault Zone from SAFOD cuttings and core. Geophys. Res. Abstr. v. 8, 05248, 2006b.
- Thayer M., Arrowsmith J. Fault Zone Structure of Middle Mountain, Central California. AGU Abstr., T21A-0458, 2005.
- Thordsen J. J., Evans W.C., Kharaka, Kennedy Y. K., van Soest M. Chemical and Isotopic Composition of Water and Gases From the SAFOD Wells: Implications to the Dynamics of the San Andreas Fault at Parkfield, California. AGU Abstr. T23E-08, 2005.
- Thurber C., Roecker S., Zhang H., Baher S., Ellsworth W. Fine-scale structure of the San Andreas fault zone and location of the SAFOD target earthquakes. GRL 31, L12S02, doi: 10.1029/2003GL019398, 2004.
- Unsworth M., Bedrosian P. A. Electrical resistivity structure at the SAFOD site from magnetotelluric exploration GRL 31, L12S05 **doi:**10.1029/2003GL019405, 2004.
- van der Pluijm B., Schleicher A. M., Solum J., Tourscher S. N., Warr L. N. Phyllosilicate mineral assemblages, elemental compositions and microstructures from the SAFOD Main Hole. AGU Abstr, T21A-0456, 2005.
- Wentworth C. M., Jachens R. C., Simpson R. W., Michael A. J. Structure of the Parkfield region, CA, from geology and geophysics compiled in a Geographic Information System, Eos Trans. AGU, 73(43), F396, 1992.
- Zoback M. D. Hickman S., Ellsworth B. Drilling, sampling, and measurements in the San Andreas Fault Zone at seismogenic depth, Eos Trans. AGU, 86(52), Abstr. T23E-01, 2005.

#### APPENDIX

# A1. Characterization recommended to NSF by an international panel (Evans et al.2004 SAFOD sample analyses workshop)

#### In-situ

Mineralogy (XRD) and petrography (optical) of cuttings and core

Downhole petrophysical measurements (e.g., Logging While Drilling)

In-situ measurements of fluid pressure and permeability

Mesostructural core description (e.g., basic lithology, core condition, fluid content, fracture orientation, density, distribution, cross-cutting relationships)

Multi-sensor track physical property logging (natural gamma logs)

Bulk magnetic susceptibility

Stress relaxation measurements

Continuous sampling for fluid chemistry (major ions)

#### Laboratory

Core reorientation (from magnetic remanence method)

Microstructural properties (including particle- and pore-size distribution, and textural analyses, microstructures, nature of mineral distribution); possibly CT scan on selected cores

Density and porosity properties

Thermal and electrical properties

Magnetic properties (anisotropy of susceptibility, magnetic mineralogy)

Frictional strength and rheological properties

Permeability and poromechanical properties

Seismic velocities and anisotropy; anelastic and attenuation behavior

Detailed core description (building on on-site description)

Elemental analysis (ICP)

Fluid chemistry (minors, stable isotopes)

CO2, CH4, noble gas analyses (from pressurized fluid samples)

Microbial activity and organic-C analysis

Vein and fluid inclusion chemistry (major and minor elements, stable isotopes)

Dating of host minerals and fault rock (U/Pb. Ar, ESR, TL dating) – these might be experimental

#### Planned real- time core measurements for phases 2 and 3

Flat scans and 360° scans of entire core whenever possible ("unwrapped" image) essential for core documentation; baseline data. 360° scans can be used with borehole image logs to orient core.

USGS scanner used (modified GeoTek system).

Continuous physical property scans - USGS GeoTek system:

P-wave velocity, density (active gamma), magnetic susceptibility and resistivity (induction).

Natural gamma and spectral gamma (U, Th, K) also possible through contractor. Core will be shrink-wrapped in non-conductive plastic D-tubes (ala. IODP) for scanning and storage.

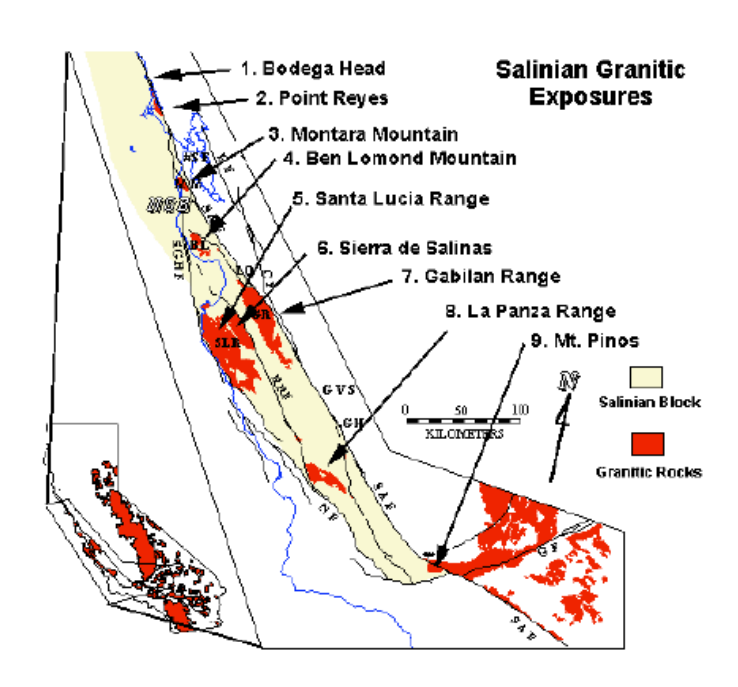
During Phase 3 (continuous coring) core processing and measurements will be done on site (mobile core lab.

#### **A2.** The Franciscan Complex

The Franciscan Complex contains high-grade metamorphic rocks that formed at great depths in a subduction zone. Blocks include amphibolites, eclogites, and blueschists that exhibit the highest grade of metamorphism of any rocks in the Franciscan. These high-grade rocks are found in a shale and serpentinite matrix mélange that give the local topography is distinctive look — large blocks of resistant metamorphic rocks in a matrix of soft, easily erodible shale and serpentinite. Minerals to look for in these rocks include garnet, amphibole, epidote, omphacite (clinopyroxene), and a blue amphibole called glaucophane. Geochronologic data indicate that the high-grade blocks are the oldest rocks in the Franciscan Complex having been metamorphosed about 160 Ma. Franciscan rocks form the east wall of the SAF for virtually its entire course through the Coast Ranges of central and northern California, although the Franciscan is concealed along some reaches of the fault by overlying rocks. The Franciscan is a heterogeneous assemblage that consists largely of dismembered sequences of graywacke, shale, and lesser amounts of mafic volcanic rocks, thin bedded chert, and rare limestone. These rocks also occur with serpentinite and tectonic pods of blueschist in mélange zones that are the locus of much shearing within the Franciscan and those generally separate blocks of the more coherent sequences. The sedimentary and volcanic Franciscan rocks were formed in a deep marine environment, as attested by the abundance of foraminifers in the limestone and by radiolarians in the chert. Most of these rocks are probably Late Jurassic and Cretaceous in age, c. 160 to 100 Ma (Bailey and others, 1964), but some of the chert and associated volcanic rocks are as old as Early Jurassic, c. 200 Ma (Irwin and others, 1977; Blome and Irwin, 1983). In the northern Coast Ranges, some of the rocks assigned to the coastal belt of the Franciscan assemblage are as young as late Tertiary and are thought to have accreted to North America during post-middle Miocene time (McLaughlin and others, 1982). The geochemistry of the basalt is consistent with formation at an oceanic spreading center – most Franciscan volcanic rocks appear to have formed at spreading ridges or were erupted off-axis at seamounts or oceanic rises. Pillow structures are occasionally visible in the basalts. As the oceanic plate moved toward the Franciscan subduction zone, greywacke was deposited on top of the chert at ~95 Ma as ocean floor rocks neared the Franciscan trench. The sequence of basalt-chert- graywacke is repeated many times at the Marin Headlands by thrust faults that formed during the underplating of the Marin headlands units. The age and origin of Franciscan mélange is problematic. Mid-Cretaceous limestone in mélange near Laytonville in the northern Coast Ranges, 225 km northwest of San Francisco, has a paleomagnetic inclination that indicates an origin several thousand kilometers to the south (Alvarez and others, 1980). Similarly, Franciscan pillow basalt about 45 km northwest of San Francisco is thought to have moved northward 19° of latitude (approx 2,000 km) from its site of origin (Gromme, 1984). These and other features indicate that some, possibly much, of the Franciscan has been transported great distances northward along the Pacific margin relative to a stable North America.

#### A3. Salinian block

The west wall of the SAF consists mainly of rocks of the Salinian block from the Transverse Ranges northward to Bodega Head. The principal rock types within the Salinian are granitic and metamorphic rocks, locally overlain by Upper Cretaceous and younger strata. The metamorphic rocks, which commonly are moderate- to high-grade gneiss, granofels, impure quartzite, and minor schist and marble, probably represent a metamorphosed thin-bedded sequence of siltstone and sandstone, with lesser amounts of shaly, marly, and calcareous strata (Ross, 1978). The stratigraphic age of the protoliths of the metamorphic rocks is not known. The plutonic rocks are mostly granite and tonalite, but they range in composition to gabbro. U-Pb-isotopic measurements on zircon in the plutonic rocks indicate that plutonic activity began about 120-105 Ma in the northwestern part of the Salinian block and migrated southeastward over a period of 40 m.y., with the youngest plutons intruding the Barrett Ridge slice about 80-75 Ma (Mattinson and James, 1985). Salinian granitoids are thought to be related to the Cretaceous Sierran granites which formed during Mesozoic subduction of the Farallon Plate beneath the western North American plate before the development of the San Andreas fault. Salinian granitoids are thought to have been displaced northward to their current position along the San Andreas fault from the southern Sierra Nevada batholith. The basement rocks of much of the According to Ross (1984), who compared the two terranes (the Sierra Nevada batholith and Salinian terrane rocks) in considerable detail, the similarities are so great that strong data would be required to support an alternative origin. Paleomagnetic data, however, indicate that the Salinian block may have been displaced 2,500 km northward since Cretaceous time (Champion and others, 1984) and that it may have originated near the latitude of Central America or Mexico in the axial part of the Cordilleran Cretaceous plutonic arc (Page, 1982).



# A4. Velocity dependence of the friction coefficient for steady-state sliding at room temperature

Rock/gouge type	Normal stress (MPa)	Velocity dependence	Maximum ∂r <sub>s</sub> ∂lnV	Slip displace- ment (mm)	Silding speed (µm s <sup>-1</sup> )	Reference
Initially bare surface						
Granite	2	-	0.009	< 10	10"1-10	Dieterich 1978, 1981
Granite	25	+	0.002	0 - 10	1-10	Beeler et al 1996
	25	-	0.005	15 - 400	1-10	
Granite	5	-	0.003	6 - 24	10 <sup>-3</sup> –1	Kilgore, Blanpied and Dieterich 1993
	5	+	0.003	6 - 24	10-103	
	30 - 150	-	0.005	6 - 24	10-2-102	
Granite	25	-	0.006	50 - 500	10-2-102	Blanpied, Tullis and Weeks 1998
	25	+	0.009	50 - 500	$10^3 - 3.2 \times 10^3$	
Granite (water saturated)	100	-	0.002	< 13	2×10 <sup>-1</sup> -10	Marone, Raleigh and Scholz 1990
Quartzite	3	-	0.009	< 10	0.01-2	Ruina 1980
Dolomite	75	+	0.005	25 - 4.7	10 <sup>-2</sup> -1	Weeks and Tullis 1985
Gabbro (smooth)	5	-	0.002	10 - 60	10-1-10	Marone and Cox 1994
Gabbro (rough)	5	-	0.006	2 - 38	10 <sup>-1</sup> _10	
	5	+	0.001	54 - 62	10 <sup>-1</sup> –10	0.1
Serpentinite (antigorite)	25 - 125	+	0.018	< 400	3.2×10 <sup>-5</sup> =3.2×10 <sup>2</sup>	Reinen et al. 1991
	25 – 125	-	0.005	< 400	10"1-10	
Crushed granite	10	+	0.004	< 25	2.5×10 <sup>-1</sup> -25	Dieterich 1981
	10	-	0.005	25 - 8	2.5×10 <sup>-1</sup> -25	
Crushed granite	25	-	0.002	20 - 60	1-10	Beeler et al. 1996
	25	+	0.004	100 - 400	1-10	
Crushed granite	50 - 600	+	0.007	< 10	7×10 <sup>-3</sup> -7	Solberg and Byerke 1984
Feldspar	25	-	800.0	30 - 170	10-3-10	Scruggs and Tullis 1998
Quartz	25 - 70	+	0.014	2 - 4	10 <sup>-3</sup> _10	Mair and Marone 1999
	25 - 70	-	0.007	8 - 16	10 <sup>-1</sup> -10	
Quartz (water saturated)	50 - 190	+	0.004	< 13	10-1-30	Marone, Raleigh and Scholz 1990
[[ite,montmori]onite, and mixture (saturated)	360 – 400	+	0.007	< 8	10~2-1	Morrow, Radney and Byerlee 1992
Quartz-montmorijonite mixture (saturated)	55- 81	+	800.0	≺ 12	3×10 <sup>-8</sup> -2×10 <sup>2</sup>	Logan and Rauenzahn 1987
Muscovite	25 - 150	+	0.006	< 200	10 <sup>-3</sup> -10	Scruggs and Tullis 1998
Biotite	25	-	0.006	< 150	10 <sup>-3</sup> -10	Scruggs and Tullis 1998
Serpentinite (antigorite, chrysotile)	25 25	<u>+</u>	0.04 0.01	< 276 < 276	10 <sup>-5</sup> -10 <sup>-1</sup> 1-32	Reinen, Weeks and Tullis 1994

A5. Resistivity image of the subsurface at the SAFOD site showing progression of the phase 1 and 2 drilling operations. Resistivities from Unsworth & Bedrosian (2004). Earthquake locations Thurber and Roecker (2004).

